FASTRAN ANALYSES OF COUPONS WITH RESIDUAL STRESSES DUE TO OVERLOADS AND COLD-WORKED HOLES

J. C. Newman, Jr., S. R. Daniewicz, J. LaRue
Mississippi State University
Mississippi State, MS, USA 39762
and
Dy Le
Federal Aviation Administration
William J. Hughes Technical Center
Atlantic City International Airport, NJ, USA 08405

Abstract

The objective of this study was to enhance the FASTRAN life-prediction model to simulate the introduction of compressive residual stresses due to cold-worked holes. The crack-closure model was previously developed to predict crack growth during variable-amplitude load spectra, which models the plastic deformations and residual stresses during changing load histories, such as after an overload. The cold-working process plastically overloads the material around the hole by inserting a mandrel of slightly larger diameter than the original hole. Once the mandrel is removed, a compressive residual stress develops at the edge of the hole. This is the same mechanism that causes plastic deformations, crack closure, and compressive residual stresses to develop at the crack front and along the crack surfaces.

Fatigue crack growth rate data generated on coupons with various forms of compressive residual stresses on two aluminum alloy materials (2024-T351 and 7075-T6) were studied. All tests were conducted on coupons with a single through crack emanating from an open hole. The specimens tested by Liu induced compressive residual stresses by a remote overload, whereas the cold-worked hole specimens (Sikorsky) induced residual stresses by cold expansion of the hole. Elastic-plastic finite element analyses of the cold-working process were used to generate residual stresses around the open hole. Overloads of specific magnitudes were then applied to the FASTRAN model to generate residual stresses that simulate those calculated from the finite element method. FASTRAN was then used to make fatigue crack growth predictions under various residual-stress fields. Predictions made by the improved FASTRAN model compared fairly well with the test results from the two aluminum alloys.

Introduction

The application of overloads on cracked structural components or cold-worked holes in structural joints induce compressive residual stresses at the crack fronts or at the edges of a hole. These compressive residual stresses greatly enhance the fatigue crack growth characteristics (crack growth retardation) and the fatigue life of these components. In the past, elastic superposition methods have been used in crack growth models to account for these effects. However, this approach assumes that the residual-stress field is unaffected by crack growth and loading history. Because crack growth involves severe plastic deformations around the crack fronts and plastic deformations along the crack surfaces, there is a possibility that the compressive residual-stress fields will diminish as the crack grows through the plastic region caused by the overload or cold working, thus negating some of the benefits of the residual stresses.

The primary objective of this study was to enhance the FASTRAN crack-closure model [1,2] to simulate the introduction of compressive residual stresses due to cold-worked holes. The crack-closure model was initially developed in the late 1970s to predict crack growth during variable-amplitude load

spectra [3], which models the plastic deformations and residual stresses during changing load histories, such as after an overload. Thus, overloads may be used to simulate the plastic deformations that are generated during the process of cold-working holes. The cold-working process plastically overloads the material around the hole by inserting a mandrel of slightly larger diameter than the original hole diameter, thus, plastically deforming the material concentrically around the hole. Once the mandrel is removed, a compressive residual stress develops at the edge of the hole due to the elastic material surrounding the hole. This is the same mechanism that causes plastic deformations, crack closure, and compressive stresses to develop at the crack front and along the crack surfaces.

Fatigue crack growth rate data generated on specimens with various forms of compressive residual stresses on two aluminum alloy materials (2024-T351 and 7075-T6) were studied. All tests were conducted on specimens with a single crack emanating from an open hole. The 2024 alloy test data was generated by Liu [4,5], and the 7075 alloy test data was generated in a previous study [6]. Liu conducted two types of tests on specimens with a central hole. First, Liu subjected the specimen to a very high overload (2/3 of the material tensile yield stress), cut an electron-discharge machine (EDM) slot into one side of the hole, and then subjected the specimen to constant-amplitude loading. Second, Liu cut an EDM slot into one side of the hole, fatigue precracked the specimen to obtain a crack of a specified length, subjected the specimen to the very high overload, and then subjected the specimen to constant-amplitude loading. In the previous study, LaRue [6] obtained specimens from Sikorsky made of 7075-T6 thin-sheet material with a central hole that had been cold worked (4.5%), reamed, and slotted with a small notch (0.25 mm in length). The specimens were then subjected to constant-amplitude loading.

The specimens tested by Liu induced compressive residual stresses by a remote overload, whereas the cold-worked hole specimens (Sikorsky) induced residual stresses by pressure loading in the hole. Elastic-plastic finite element analyses of the cold-working process [6] were used to generate residual stresses around the open hole before and after reaming the hole. Overloads of specific magnitudes were then applied to the FASTRAN model to generate residual stresses that simulate those calculated from the finite element method. Comparisons were made between residual stresses calculated from both the finite element method and the crack-closure model. FASTRAN was then used to make fatigue crack growth predictions under the various residual-stress fields. Predictions made by the improved FASTRAN model were compared with experimentally measured fatigue crack growth behavior under the prescribed residual-stress fields.

FASTRAN Life-Prediction Model

During the past two decades, the FASTRAN life-prediction code has been successfully used to predict the fatigue crack growth lives for a wide variety of materials under a wide range of load histories (constant-amplitude and spectrum loading), see References 7 to 12. Using the baseline fatigue crack growth rate data for the material of interest over a wide range in stress ratios and in rates from threshold to near fracture, the code has been able to predict the fatigue crack growth rate behavior under a variety of load histories. The FASTRAN model is based on plasticity-induced deformations around a crack front and the crack-closure concept [13].

Residual stresses are induced by various forms of plastic deformation, such as cold working and shot peening. Thus, it would be a natural extension of the crack-closure model to simulate the residual stresses through plastic deformation. The model would naturally change the residual-stress distribution due to the applied loading and crack growth. Current methods, such as linear superposition, which are used to account for the influence of residual stresses on crack growth, do not account for any decay in the residual-stress field with crack growth [14].

The FASTRAN crack-growth closure model, shown in Figure 1, is based on the strip yield model concept of Dugdale [15], but modified to leave residual-plastic deformation along the crack surfaces. The plastic zone size, ρ, (region 2) is composed of plastic elements that model the crack tip plastic deformations and supports the flow stress of the material. Three-dimensional effects on the flow stress are approximated by using a constraint factor, α, which ranges from 1 (plane stress, very thin sheets) to 3 (plane strain, very thick plates). As the crack grows, plastically deformed material is left along the flank

of the crack (region 3). During cyclic loading, these elements may come into contact (close) and some may yield in compression, especially those near the crack tip. During crack growth and cyclic loading, these elements form the residual-plastic deformations that support crack closure. The crack-opening stress level, S_{op}, at which the crack tip opens, is calculated from the contact stresses. Once the crack tip opens, the very high strain concentration at the crack tip causes damage on the crack-tip element and the crack extends. The effective stress range, $\Delta S_{eff} = S_{max} - S_{op}$, is used to calculate the effective stress-intensity factor range (ΔK_{eff}), which controls the amount of fatigue-crack growth.

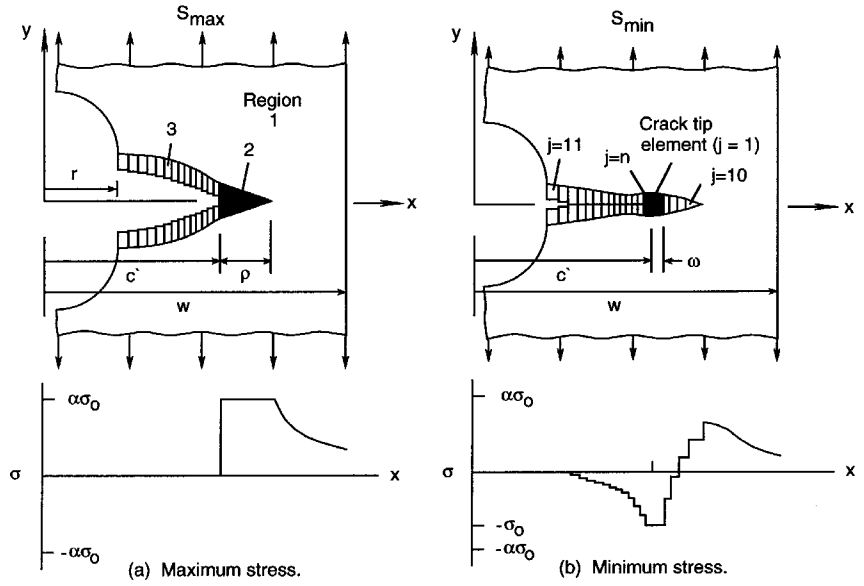

Figure 1 – Schematic of the FASTRAN crack-closure model for cracks emanating from a hole.

The FASTRAN model is used to correlate large crack growth rate data on a particular material over a very wide range in rates from threshold to fracture. From this correlation, a baseline ΔK_{eff} against rate curve is generated for the material and environmental condition of interest. (The ΔK_{eff} is the stress-intensity factor range calculated from $K_{max} - K_{op}$.) These relationships have been obtained for a wide range of materials (aluminum alloys, titanium alloys, and steels).

Model Enhancements

To more accurately model crack growth and the residual stresses due to overloads and cold-worked holes, the following modifications were made to the FASTRAN code.

(1) K-analogy was activated for all crack configurations in the current version of FASTRAN. The FASTRAN code has two basic models: one for a central crack in a finite-width plate and one for two-symmetric cracks emanating from a circular hole in a finite-width plate. The model for a crack growing from a hole is shown in Figure 1. To model a crack growing in a plate or from a hole in a different configuration and under different loading conditions than the model(s), the concept of K-analogy [2,16] is used to transfer the crack-opening stress information from the model to the actual crack configuration.

(2) The plastic zone region in the model (region 2 in Figure 1) was refined to have 20 elements in the plastic zone instead of 10. Ten elements were used in the original model to save computer time. However, it has been shown that 10 elements give essentially the same crack-opening stress results as 20 elements, but the 20-element model was used to more accurately simulate the residual-stress distributions, which exhibit very high stress gradients.

(3) The crack growth element size in the model was reduced to 5% of the cyclic plastic zone size. An element size of 20% of the cyclic plastic zone was used in the original model to save computer time. The reduced element size will make the crack-closure calculations for high stress ratios fatigue loading more accurate. But the computer speed will be reduced by a factor of about 4 from the original model. However, the advances that have been made in computer technology during the past few decades will still allow rapid crack-closure calculations using the improved model.

(4) For cracks emanating from a hole or notch, the hole-(or notch)-radius-to-plate-thickness ratio should control constraint, i.e., the elevation of the material flow stress due to multiaxial stress states. In the original model, the crack was assumed to always control the constraint level, whether the crack was growing from a hole or in a plate. This approach was done for simplicity, and the results were generally conservative. However, to improve the life calculations for a crack growing from a hole, the hole-radius-to-thickness ratio will control constraint, and on the first load cycle the state-of-stress is nearly plane stress. This will cause more yielding at the hole than in the original model, but will simulate more accurately the state of yielding at an open hole, which will have lower constraint than a crack.

(5) The stress-intensity factor solution for a single crack at an open hole in a finite plate (finite width and height) was recalculated using the FADD2D code [17] and the current solution in FASTRAN for remote uniform stress was verified as being very accurate (± 0.2%). However, the test specimen used for the cold-worked hole experiments was gripped in friction grips, which impose a more uniform displacement boundary condition on the specimen. The stress-intensity factor solution for remote uniform displacement applied to the particular test specimen configuration indicated that the stress-intensity factors were lower than the uniform stress case for cracks greater than about 1/2 of the ligament from the hole to the edge of the plate.

(6) The basic FASTRAN model for two-symmetric cracks emanating from an open hole was modified to allow reaming of the hole to increase the hole radius and to remove some of the plastically deformed material caused by cold working. The plastically deformed material from the reamed hole was transferred to a new set of model elements in the plastic zone region. Thus, reaming has modified the residual stresses induced by the original cold working.

(7) Similar to the reaming option, an option was developed to induce a cut or notch, like an EDM notch, at the edge of the hole, which would also eliminate some of the plastic-deformed material.

Test Specimens

The test specimens used in this study are shown in Figure 2. The middle-crack tension specimen, M(T), was used to obtain the basic fatigue crack growth rate data on the two materials. The specimen with the central hole was used in the studies of the various residual-stress distributions. The latter specimen was subjected to either remote uniform stress (S) or remote uniform displacement (δ).

Uniform Remote-Applied Stress

The stress-intensity factor (K_s) for a single crack emanating from an open hole in a finite-width plate subjected to a remote uniform stress is given by

$$K_s = S \sqrt{(\pi a)}\, F_{hs} \qquad (1)$$

where S is the remote-applied stress, a is the crack length measured from the hole, and F_{hs} is the boundary-correction factor, which accounts for the influence of the hole and finite-width plate. The function F_{hs} is given by

$$F_{hs} = F_n F_w \tag{2}$$

$$F_n = 0.707 + 0.765\ \lambda + 0.282\ \lambda^2 + 0.74\ \lambda^3 + 0.872\ \lambda^4 \tag{3}$$

where $\lambda = 1/(1 + a/r)$ for $0 < \lambda \leq 1$. Equation (3) is within 0.2 percent of the results in Reference 18. The finite-width correction, F_w, is given by

$$F_w = \{sec[\pi/2\ (r + a/2) / (w - a/2)]\}^{1/2} \tag{4}$$

which agrees well with Isida's solution [19,20] for an eccentric crack in a finite-width plate. Note that the crack length in Isida's crack configuration, 2a, is assumed to be equal to the crack length, a, plus the hole diameter ($a + 2r$) in Figure 2.

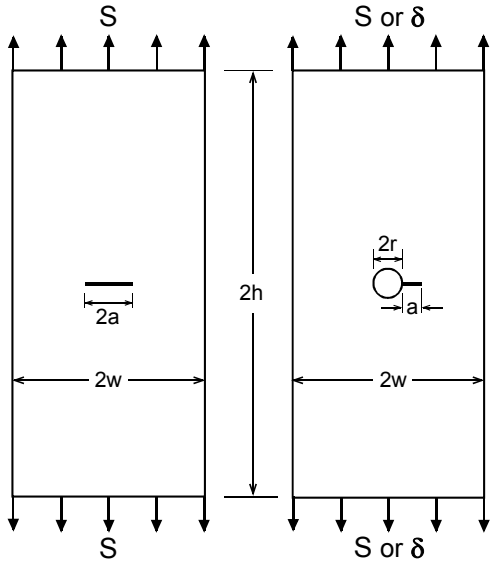

Figure 2 – Crack configurations tested and analyzed.

Uniform Remote-Applied Displacement

The stress-intensity factor (K_d) for a single crack emanating from an open hole in a finite-width plate subjected to a remote uniform displacement is

$$K_d = S \sqrt{(\pi a)}\ F_{hd} \tag{5}$$

where S is the remote-applied stress due to a uniform displacement, δ, a is the crack length measured from the hole, and F_{hd} is the boundary-correction factor, which accounts for the influence of the hole, finite-width, and finite height of the plate. The function F_{hd} is given by

$$F_{hd} = F_n F_w F_d \tag{6}$$

where F_n and F_w are given by equations (3) and (4), respectively. The function F_d accounts for the influence of the uniform-applied displacement and is a function of hole radius, specimen width, and specimen height. Herein, the function F_d was developed for only $r/w = 0.143$ and $h/w = 2$, the values used in the current test program. The function F_d is given by

$$F_d = 1 - 0.2\ \beta^2 - 0.1\ \beta^3 - 0.05\ \beta^{16} \tag{7}$$

where $\beta = (a + r)/w$. Equation (7) is within 0.5 percent of the results calculated from the boundary-element code, FADD2D [17].

Figure 3 shows a comparison of the boundary-correction factor, F_h, for uniform remote-applied stress or uniform remote-applied displacement as a function of the normalized crack length, $(a+r)/w$. The solid and open symbols show the recent results calculated from the FADD2D [17] code on the specific crack configuration with $r/w = 0.143$ and $h/w = 2$. The solid and dashed curves are the results of equations developed by Newman [7] and in the NASGRO code [21], respectively, which agreed very well with each other. The dash-dot curve is the equations developed herein (Eq. 6) for the case of uniform applied displacement. Figure 4 shows the ratio of the stress-intensity factor for the uniform displacement case to that for the uniform stress case (Eq. 7). These results demonstrate that the stress-intensity factor is greatly reduced for the larger crack-length-to-width ratios.

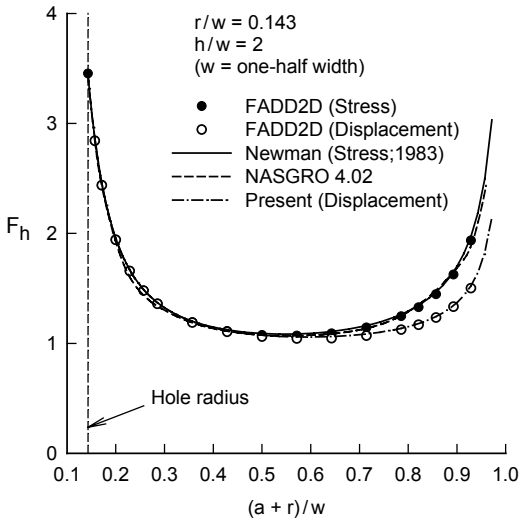

Figure 3 – Stress-intensity factor solutions for a single crack at an open hole in a finite plate.

Materials

Fatigue crack growth rate data on the two materials were obtained from the literature. The data on the 2024-T351 alloy were obtained from the Liu report [5], whereas the data for the 7075-T6 alloy were obtained from reports from NASA [22,23].

Aluminum Alloy 2024-T351

The fatigue crack growth rate data for the 2024 plate (B = 6.35 mm) is shown in Figure 5 for stress ratios ranging from $R = 0.1$ to 0.7. (The yield stress was 372 MPa, and the ultimate tensile strength was 490 MPa.) For a given ΔK value, the higher R ratio results exhibit faster crack grow rates than the low R ratio results. The solid curve shows the effective stress-intensity factor range (ΔK_{eff}) versus rate relationship for a thin-sheet 2024-T3 material [10]. These results were obtained from an analysis of Hudson's [22] and Phillips' [24] data. The ΔK_{eff} curve is the results for a fully open crack, and these results should agree with the high R ratio data, such as $R = 0.7$.

Figure 6(a) shows a crack-closure analysis of Liu's data, which shows ΔK_{eff} versus rate using the crack-opening stress equations developed from FASTRAN analyses [25]. For rates lower than 10^{-9} m/cycle, the plate material was assumed to agree with the thin-sheet material (dashed curve). And for rates greater than 10^{-5} m/cycle, the plate material was, again, assumed to agree with the thin-sheet material and match a point taken from a K_R curve on 6-mm-thick material (NASGRO database). (The extremely high rate relationship was needed to model the large amount of crack extension exhibited in the test specimen that was fatigue precracked and then overloaded to 2/3 of the material yield stress.

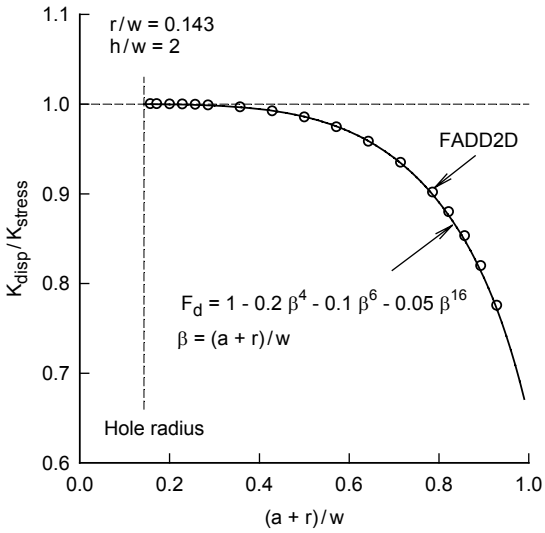

Figure 4 – Ratio of stress-intensity factors for uniform displacement to uniform stress for a single crack at an open hole in a finite plate.

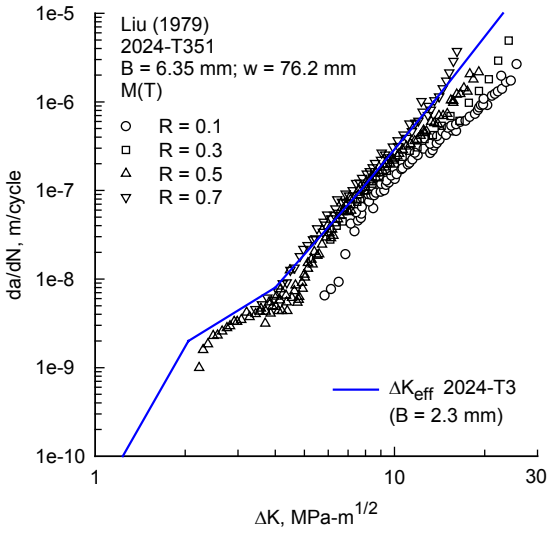

Figure 5 – Fatigue crack growth rate versus stress-intensity factor range for 2024-T351 plate at various stress ratios.

Cracks growing in thin sheets and plates show a flat fatigue crack surface at low rates and, usually, a slant (45°) fatigue crack surface at high rates. The transition from flat-to-slant crack growth is characteristic of a constraint loss, in that the constraint changes from plane strain to plane stress during the transition. The vertical dashed line (Fig. 6a) shows the transition location in terms of ΔK_{eff} that was calculated using an equation developed in Reference 10, $(\Delta K_{eff})_T = 0.5\ \sigma_o \sqrt{B}$. The data correlated within a fairly tight band, except in the region around 10^{-7} m/cycle. Here, some spread in the data was apparent as a function of the R ratio. The baseline curve (solid curve with open symbols) was chosen to fit the average of these data. Normally, the high R ratio results, such as 0.7, are used to obtain the ΔK_{eff}-rate relationship. The results for only $R = 0.7$ are shown in Figure 6(b). Note that the $R = 0.7$ data falls in between the thin sheet and the current baseline relation. The results for only $R = 0.1$ are shown in Figure 6(c). The low R data is significantly higher than the baseline curve around a rate of 10^{-7} m/cycle.

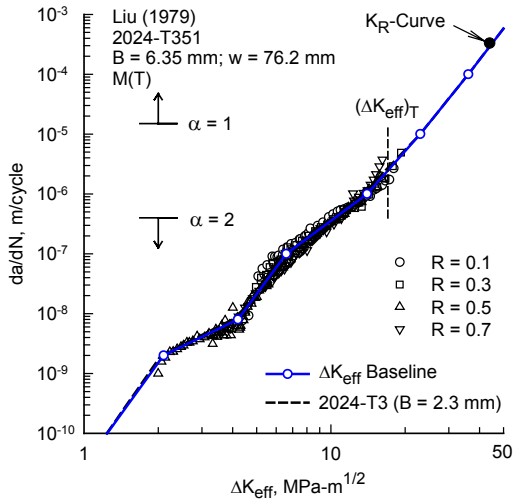

Figure 6(a) – Effective stress-intensity factor range versus rate for 2024-T351 plate.

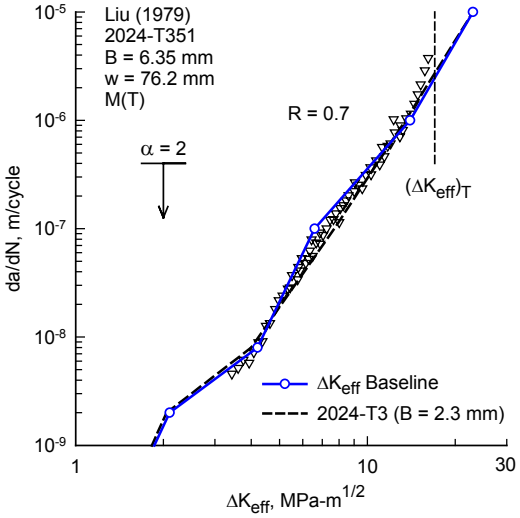

Figure 6(b) – Effective stress-intensity factor range versus rate for 2024-T351 plate for $R = 0.7$.

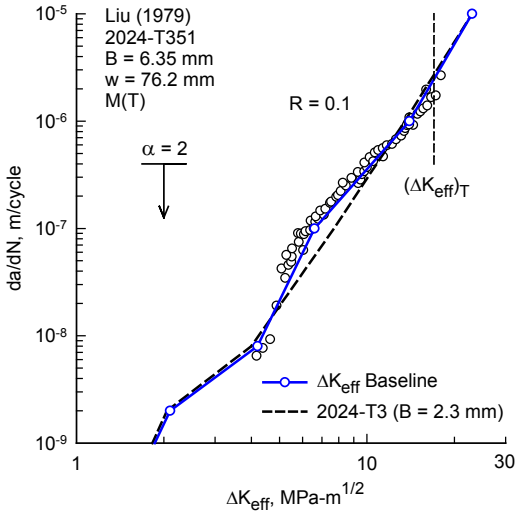

Figure 6(c) – Effective stress-intensity factor range versus rate for 2024-T351 plate for $R = 0.1$.

The baseline effective stress-intensity factor versus rate relationship used in the FASTRAN code is shown by the solid lines with open symbols in Figure 6. A table-lookup form with a simple power law relation is used between each data point, as shown by the lines between each data point. The table-lookup form is used because many materials show transitions in rates at various locations along the curve. These transitions have been associated with microstructure and environment. The baseline relation for the 2024-T351 alloy is given in Table 1.

Table 1 – Effective Stress-Intensity Factor Versus Rate Relationship for 2024-T351.

ΔK_{eff}, MPa-m$^{1/2}$	da/dN, m/cycle
0.80	1.00e-12
1.10	5.00e-11
2.05	2.00e-9
4.00	8.00e-9
7.70	1.00e-7
13.5	1.00e-6
23.0	1.00e-5
36.0	1.00e-4
85.0	1.00e-2
$\alpha = 2.0$	4.00e-7
$\alpha = 1.0$	1.50e-5

Aluminum Alloy 7075-T6

An effective stress-intensity factor versus rate relationship had previously been obtained on the thin-sheet 7075 alloy [10,23]. (The yield stress was 520 MPa and the ultimate tensile strength was 575 MPa.) Figure 7(a) shows this correlation on the data generated in Reference 23. The data generated for three stress ratios correlated extremely well, except in the near-threshold regime. The baseline relation is fitted to the mean of these data, as shown by the solid curve with solid symbols. The solid symbols are the table-lookup values used in the FASTRAN code. Again, the flat-to-slant crack growth regime (constraint loss regime) was defined and the values of constraint (α) were established from variable-amplitude load tests in Reference 23. The location and constraint values for the constraint loss regime are best established using variable-amplitude fatigue crack growth rate tests instead of constant-amplitude tests. Figure 7(b) shows another data set on the 7075 alloy. Hudson obtained these data in 1969 [22], which exhibited some differences in the high-rate regime. For rates less than about 10^{-9} m/cycle, the baseline curve (solid curve and solid symbols) was fit to small crack data [23] and this relationship will be used herein. In Figure 7(b), the solid lines show the baseline effective stress-intensity factor versus rate relation used in the FASTRAN code for the 7075-T6 material and is given in Table 2.

Overload Tests

The tests conducted by Liu [4,5] were analyzed with the improved FASTRAN for three loading conditions. First, crack growth predictions are made under constant-amplitude loading on M(T) specimens; second, the preyielded holes, and third, the precracked and overload holes were analyzed. Comparisons are made between test and analyses for many of the test conditions reported by Liu.

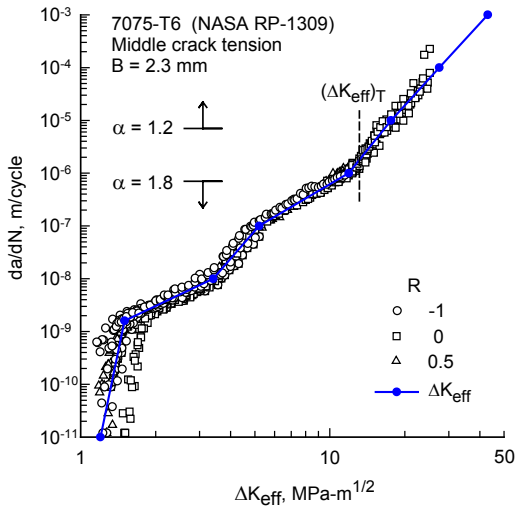

Figure 7(a) – Effective stress-intensity factor range versus rate for 7075-T6 sheet for various stress ratios on small M(T) specimens.

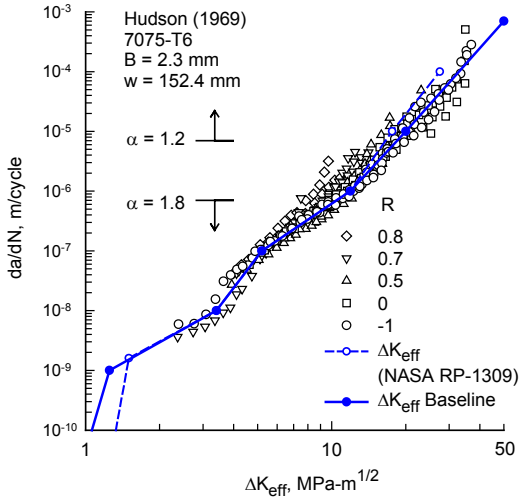

Figure 7(b) – Effective stress-intensity factor range versus rate for 7075-T6 sheet for various stress ratios on large M(T) specimens

Table 2 – Effective Stress-Intensity Factor Versus Rate Relationship for 7075-T6.

ΔK_{eff}, MPa-m$^{1/2}$	*da/dN*, m/cycle
0.90	1.00e-11
1.25	1.00e-9
3.40	1.00e-8
5.20	1.00e-7
11.90	1.00e-6
20.0	1.00e-5
50.0	7.00e-4
$\alpha = 1.8$	7.00e-7
$\alpha = 1.2$	7.00e-6

Constant-Amplitude Loading

Figure 8 shows the measured and calculated crack length against cycles on two M(T) tests conducted at two remote-applied stress levels at $R = 0.1$. The symbols show the tests and the curves show the calculations. The discrepancy (50% on final life) is partly due to the correlation shown on Figure 6(c), which shows that the measured rate data is faster than the baseline relationship. However, the initial rates observed on the test data (first two data points) did not agree with the ΔK-rate data (open circles) shown in Figure 6(c), so these data may be questioned. Further study would be required to resolve this discrepancy.

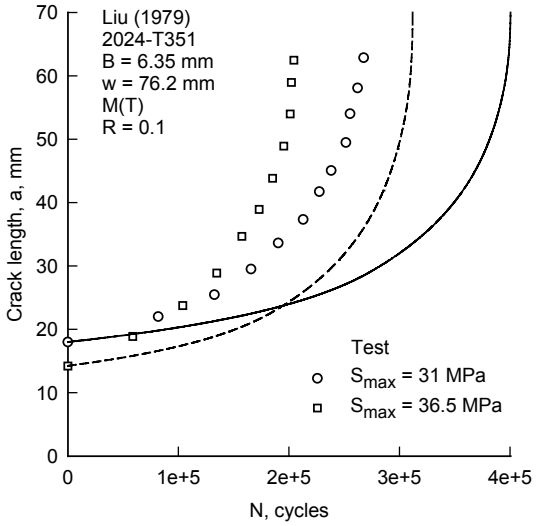

Figure 8 – Measured and calculated crack length versus cycles on M(T) specimens made of 2024-T251 alloy under constant-amplitude loading.

Preyielded Hole and Constant-Amplitude Loading

As previously mentioned, FASTRAN has always modeled yielding that occurs at the edge of a hole using the strip yield model [7], as shown in Figures 9(a) and 9(b). As seen, the modified Dugdale model does not simulate the two-dimensional nature of the yield zone at a hole or even at a crack. But the model has been successful in modeling crack growth behavior under various load histories as an engineering tool. However, on the initial overload, the state of stress is now assumed to be nearly plane stress, whereas the crack may be growing under a high constraint condition, like plane strain. This lower constraint will cause more yielding to occur in the crack-closure model at the edge of the hole. After the overload, an EDM notch is machined into one side of the hole of length, a_i, as shown in Figure 9(c). The simulation in FASTRAN is shown in Figure 9(d). The EDM notch removes some of the plastically deformed material at the edge of the hole.

Figures 10(a) to 10(c) show comparisons made between the tests and analyses made with FASTRAN. The plots show log crack length versus linear cycles, so that the unique behavior of the test and analyses can be observed in the small crack regime. (Note that a linear plot of crack length versus cycles will not show any distinction between constant-amplitude and preyielded hole results in the early stages of crack growth, i.e., the curves are extremely flat.) The solid and dashed curves are the predictions made with FASTRAN for the preyielded and no overload cases, respectively. FASTRAN was able to accurately describe the influence of the compressive residual stresses on crack growth for all of the test cases. These results show that there is very little difference in total life between the no overload and the preyielded condition, but the shape of the crack length versus cycles curves are distinctly different in the early stages of crack growth. The results shown in Figures 10(a) to 10(c) indicate that the

model predicts a slightly longer life that the tests for the smaller EDM cut. Further study would be required to resolve this issue.

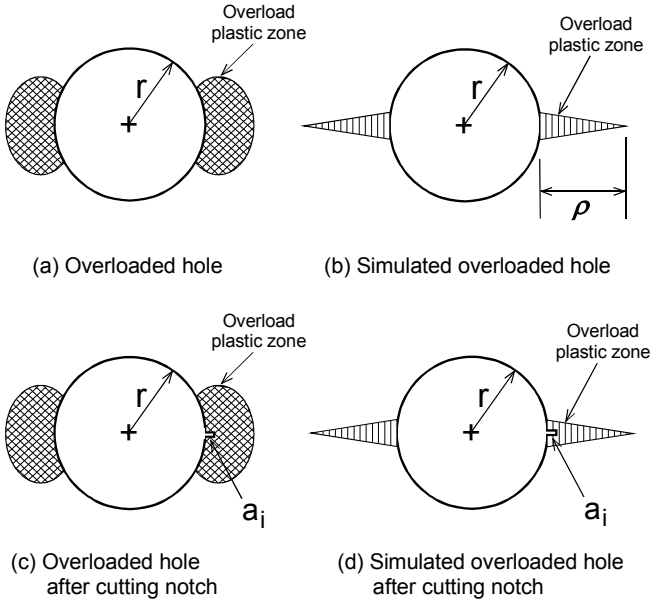

Figure 9 – Preyielded hole with overload and simulated behavior in FASTRAN.

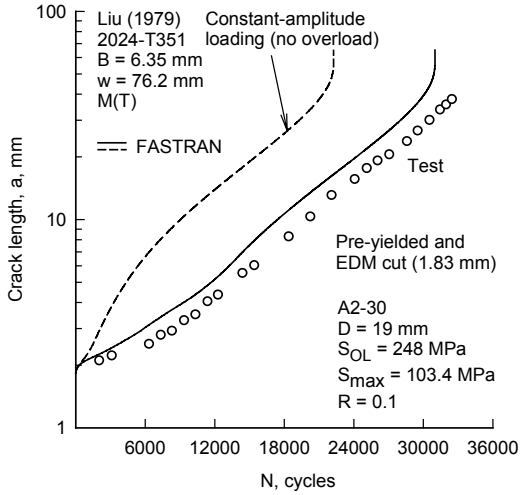

Figure 10(a) – Measured and predicted crack length versus cycles under constant-amplitude loading after a preyielded hole was EDM cut with 1.83-mm notch.

Precracked, Overloaded, and Constant-Amplitude Loading

Several specimens made of the 2024 alloy were EDM cut on one side of the hole, fatigue precracked to a specified initial crack length, a_i, under constant-amplitude loading, and then the specimen was severely overloaded to 248 MPa (2/3 of the yield stress of the material). Figure 11 shows the comparison between a test (A2-25) and the FASTRAN simulations. The solid and dashed curves show the overload and no-overload cases, respectively. In this case, there was nearly a factor of 2 difference between the no-overload predictions and the test results. However, FASTRAN predicted that the crack in the precracked and overloaded case (solid curve) would grow and nearly stop (failure predicted at 260,000 cycles).

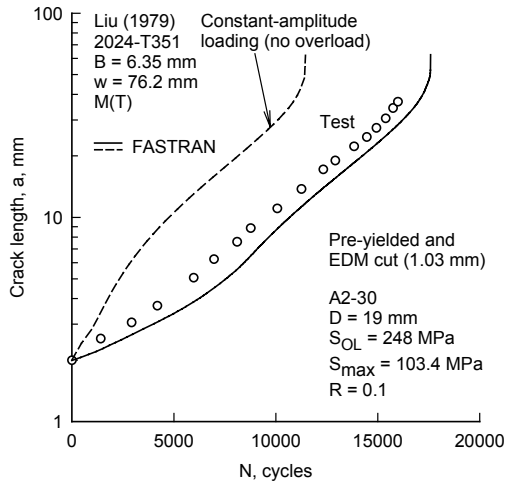

Figure 10(b) – Measured and predicted crack length versus cycles under constant-amplitude loading after a preyielded hole was EDM cut with 1.03-mm notch.

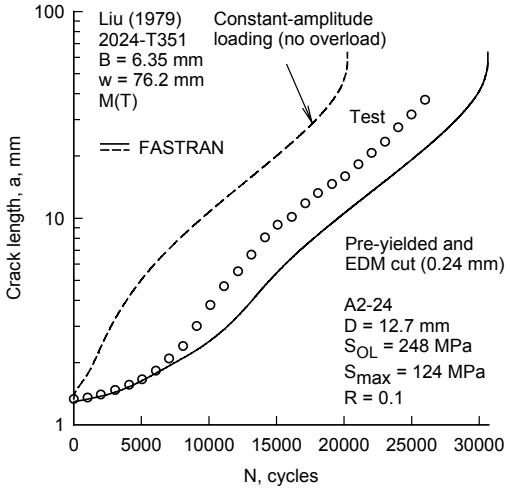

Figure 10(c) – Measured and predicted crack length versus cycles under constant-amplitude loading after a preyielded hole was EDM cut with 0.24-mm notch.

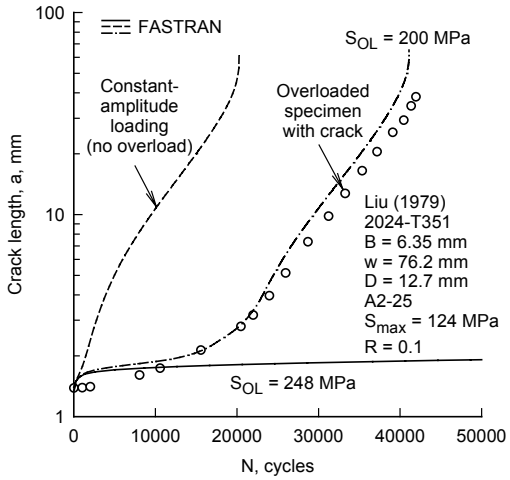

Figure 11 – Measured and predicted crack length versus cycles under constant-amplitude loading after an EDM notch was made at a hole, fatigue precracked, and then overloaded.

This type of behavior has been observed in past experiments on fatigue crack growth. Hudson and Hardrath [26] observed that after a maximum stress change from 200 to 100 MPa (R = 0), a crack would grow and stop while another crack would initiate along the fatigue crack surfaces (perpendicular to the main crack) and grow around the plastic zone size created during the higher stress amplitude.

A schematic of the anticipated crack behavior in the precracked and overloaded case is shown in Figure 12. After fatigue precracking to an initial crack length of a_i, the specimen was overloaded to 248 MPa. The solid circle (denoted K_R-curve) shown in Figure 6(a) represents the predicted crack extension during the overload. Thus, the specimen was in the fracture process and the crack would have developed along shear bands (70^o) to the plane of the precrack, i.e., forming the slant fracture behavior through the plate thickness. The plastic zone sizes are scaled to approximate sizes compared to the hole radius. Thus, the crack would have grown around the primary plastic zone caused by the overload and the crack-closure behavior would have been dramatically reduced from the FASTRAN predictions. FASTRAN, as in the case of the Hudson-Hardrath test, forced the crack to grow self-similar along the dashed line into the overload plastic zone. However, the crack-opening stress levels would reach very high levels and produce extremely slow crack growth rates. In summary, FASTRAN has not been programmed to model this unique behavior during severe stress amplitude changes, which result in difference fracture modes.

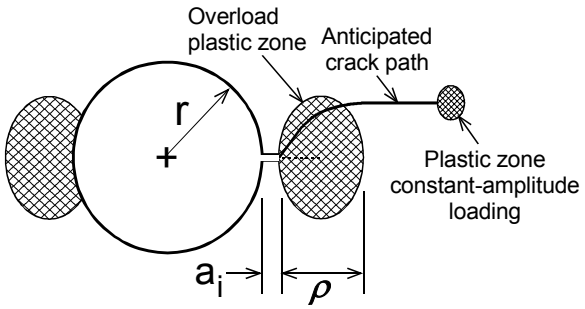

Figure 12 – Anticipated crack path in the precracked specimen during and after the overload.

Thus, a trial-and-error procedure was used to find an overload that would cause FASTRAN to fit the final life in the test case. Here, it was found that an overload of 200 MPa would fit the results very well. It would be of future interest to conduct these type of tests and vary the overload to see if FASTRAN could predict the behavior for self-similar crack growth or to modify FASTRAN to simulate the fracture process and reduce the residual plastic deformation along the anticipated crack path.

Cold-Worked Hole Tests

The tests conducted by LaRue [6], using cold-worked specimens obtained from Sikorsky, were analyzed with the improved FASTRAN code for two loading conditions. First, crack growth predictions are made under constant-amplitude loading on single-crack-at-an-open-hole specimens. Second, the cold-worked, reamed, and notched specimens were analyzed. Comparisons were made between all of the tests and the predicted results from FASTRAN.

Constant-Amplitude Loading

Figure 13 shows the measured and predicted crack length versus cycles results on two test specimens conducted at two different remote-applied stress levels at R = 0.1. The symbols show the tests and the curves show the predictions. Here, the results are presented as a log-log plot so that both test and analyses can be shown on the same plot, because there is over an order-of-magnitude difference in the test lives. Both test specimens had an initial crack length of 0.25 mm in length from one side of the central hole. The predicted results agreed extremely well with the test data.

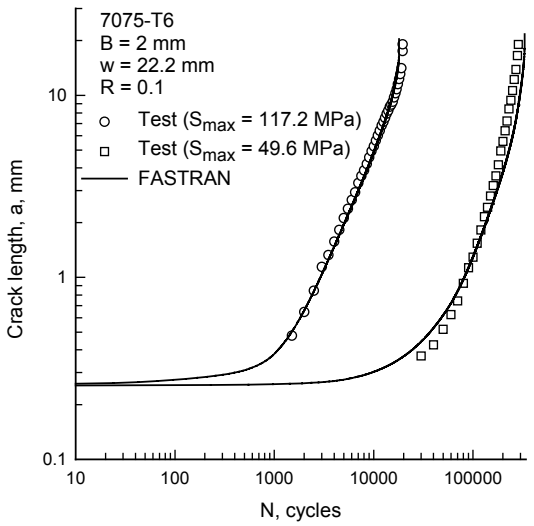

Figure 13 – Measured and predicted crack length versus cycles under constant-amplitude loading for single-crack-at-an-open-hole specimens made of 7075-T6 alloy at two applied stress levels.

All the constant-amplitude tests conducted at the higher stress level (117.2 MPa) are shown in Figure 14. Again, the initial crack lengths had an average value of 0.25 mm in length. Two predictions were made with FASTRAN. First, predictions were made for the uniform-applied stress case (dashed curve). These results indicated that something was causing the predicted results to produce much higher crack growth rates than the tests for crack lengths greater than about 6 mm. At this point, the remote boundary conditions on the test specimen were under question. It was known that remote displacement boundary conditions for an un-symmetrical crack configuration would cause a load transfer to the stiffer ligament that would lower the stress-intensity factors for the cracked ligament. Thus, the FADD2D code [17] was used to generate the stress-intensity factor solution for the remote uniform displacement case. Using these results produced the solid curve in Figure 14. The predicted results are now in better agreement with the test data, but still fall short. It is suspected that there may be something else in the specimen gripping or in the load train that would further reduce the stress-intensity factors.

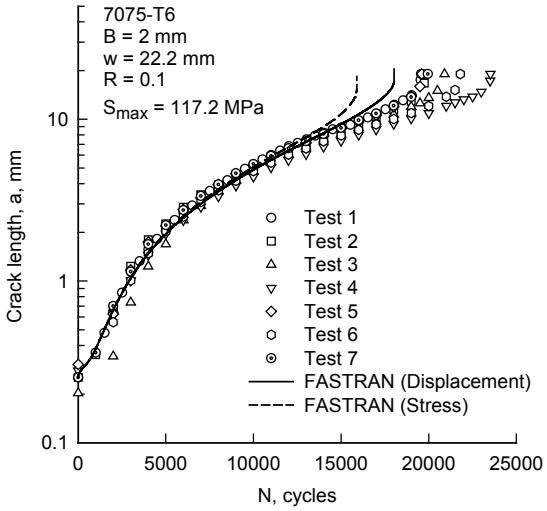

Figure 14 – Measured and predicted crack length versus cycles under constant-amplitude loading for several single-crack-at-an-open-hole specimens made of 7075-T6 alloy.

Cold-Worked and Constant-Amplitude Loading

To simulate cold-worked and reamed holes in FASTRAN required significant modification. The cold-working process plastically overloads the material around the hole by inserting a mandrel of slightly larger diameter than the original hole diameter, r. The plastically deformed material (or yield zone) forms concentrically around the hole, as shown in Figure 15(a). Once the mandrel is removed, a compressive residual stress develops at the edge of the hole due to the elastic material surrounding the hole. In the current study, overloads of specific magnitudes are applied to the FASTRAN model to generate a plastic zone region and compressive residual stresses that simulate those produced during the cold-working process, as shown in Figure 15(b). In the case of an overload, previously discussed, the modified Dugdale model does not produce the type of yielding that is produced during the cold-working process. Whether or not the simple model can be used with remote overloads to simulate the compressive residual stresses produced during cold working are studied. (A similar model could also be developed, which would pressurize the hole, similar to cold working. This model may produce a different residual plastic deformation region, but this would require further study, if the overload method was unsatisfactory.) This approach does require a calibration between either finite-element analyses (see Ref. 6) or some of the closed-form equations that have been developed for cold working (see Refs. 27 and 28). Comparisons will be made between the residual stresses calculated from both the finite element method [6] and the crack-closure model.

In addition, the cold-worked hole was reamed to a radius of r_m. The reaming of the hole removed a large amount of the plastically deformed material at the edge of the hole and greatly reduced the extent of the compressive residual stresses. After reaming the hole, an EDM notch was machined into one side of the hole of length, a_i, as shown in Figure 15(c). The EDM notch, again, removed some plastically deformed material at the edge of the hole. The simulation in FASTRAN is shown in Figure 15(d).

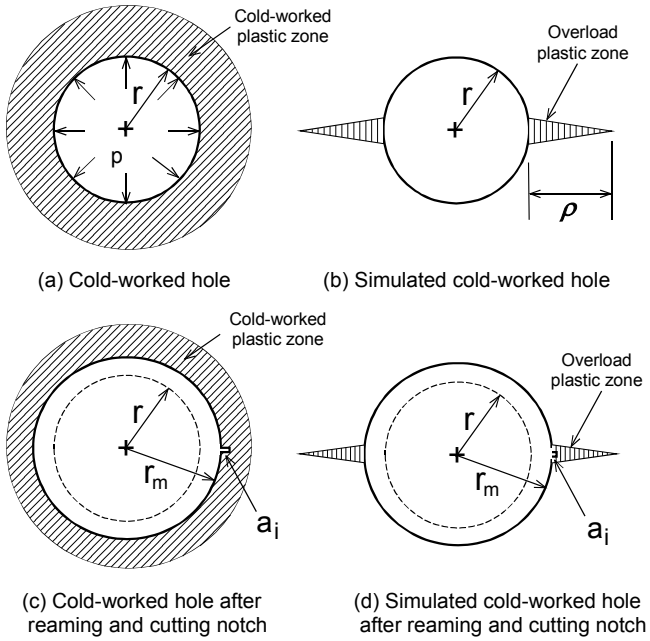

Figure 15 – Cold-worked hole and simulated behavior in FASTRAN.

A finite element code was used to analyze a cold-worked hole in the test specimen shown in Figure 2 (without a notch or crack). The specimen width (w) was 21.6 mm and the specimen was friction gripped with an h/w ratio of about 2. The details of the analysis are given in Reference 6. The initial radius (r) was about 3 mm. A mandrel with diametrical interference of 0.268 mm, corresponding to 4.5% cold expansion, was pulled through the hole to induce the compressive residual-stress field. In the final

specimens, the hole was reamed to a radius of 4.37 mm to relieve some of the residual stresses around the hole.

The normalized residual stress (σ_{rs}/σ_{ys}), as a function of the distance from the hole (x/r), is shown in Figure 16 as open symbols. The tensile yield zone had extended to about twice the hole radius; and the reverse plastic zone was about 20% of the hole radius. Various tensile overloads (S_{OL}) were applied to the crack-closure model and the resulting residual-stress distributions are shown as the curves. The end of each curve shows the extent of the tensile plastic zone. The 350 MPa overload matched the tensile plastic zone, but did not produce enough compressive residual stresses in the plastic zone. The solid curve at 420 MPa tended to match the reverse plastic zone size and approximated the residual-stress distribution on the average. The latter overload will be used to simulate the cold-worked hole.

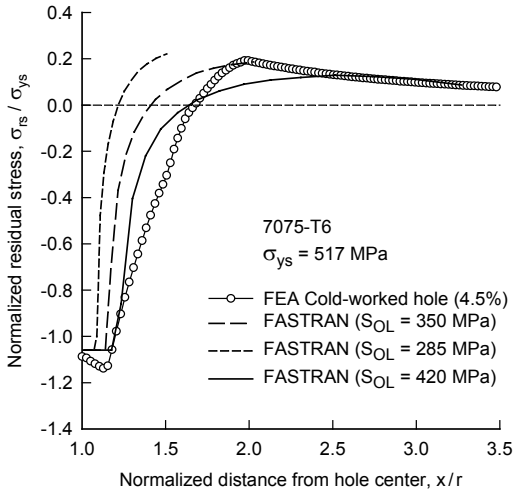

Figure 16 – Normalized residual-stresses for cold-worked hole from FEA and simulated behavior in FASTRAN.

The finite element analysis (FEA) was also used to simulate the process of reaming and notching the hole in the cold-worked specimen. The normalized residual stress, as a function of the distance from the hole, is shown in Figure 17 as open symbols. The circular symbols show the final residual-stress distribution predicted to be present in the test specimens [6]. Again, the curves show the results of the reaming and notching simulations in FASTRAN. The solid curve (420 MPa) tended to match the residual- stress distribution fairly well. Figure 18 shows the residual plastic deformations in the crack-closure model after the overload (solid symbols) and after reaming the hole (open symbols) as a function of the distance to the tip of the tensile plastic zone (x/d_{max}). The reaming process greatly reduced the amount of plastic deformation from the cold-worked hole.

The cold-worked and reamed holes were then notched with a 0.25 mm length cut on one side of the hole and the specimens were subjected to a constant-amplitude loading (S_{max} = 117.2 MPa; R = 0.1). The results of four tests are shown in Figure 19 as symbols. The initial crack length for each specimen is shown at 100 cycles. The cycles required to initiate a crack at the notch, which is estimated to be less than a few thousand cycles, is included in the crack length versus cycles data. The dashed curve shows the predicted results for only constant-amplitude loading (no cold working), but using the larger hole radius and same initial notch size. The solid curve shows the predicted results from FASTRAN, which was about 45% short of the average of the four tests. In view of the fact that the residual stresses in the FASTRAN model (Figs. 16 and 17) were less than those from the finite element analyses, the comparison was reasonable. The modified FASTRAN predicted the nearly order-of-magnitude enhancement in life due to cold working. Further study is needed to improve the residual stresses caused by cold working in the model.

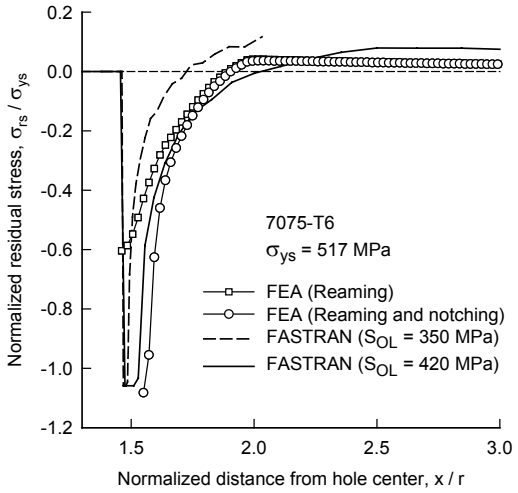

Figure 17 – Normalized residual stresses after reaming and notching cold-worked hole from FEA and simulated behavior in FASTRAN.

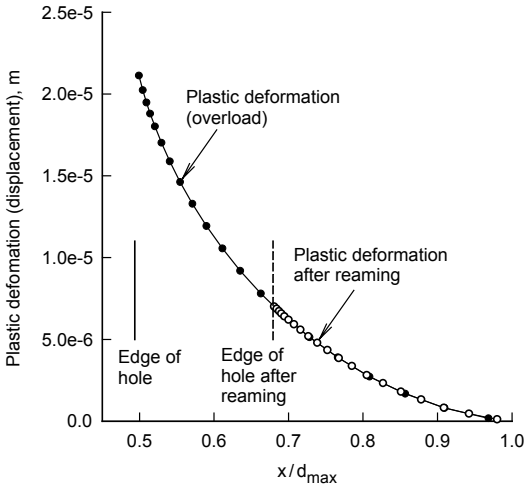

Figure 18 – Residual plastic deformations in FASTRAN during simulated cold working and reaming.

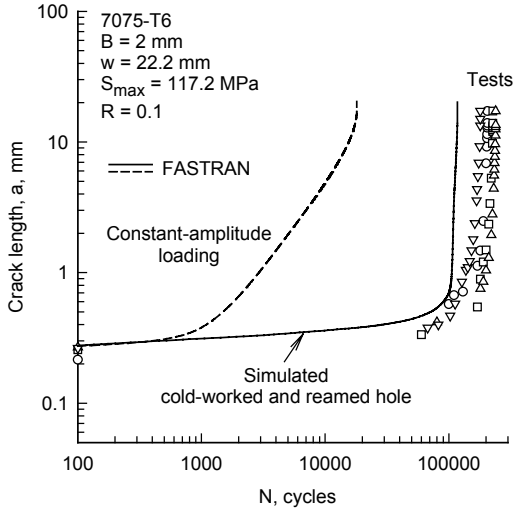

Figure 19 – Measured and predicted crack length versus cycles under constant-amplitude loading after cold working, reaming, and notching.

The enhancement from the crack-closure model was due to the higher crack-opening stress levels generated in the cold-worked and reamed specimens. Figures 20(a) and 20(b) show the crack-opening stress ratio as a function of either crack length or cycles, respectively. The dashed curve shows the calculated crack-opening stress ratio under constant-amplitude loading (no cold working). The rise in the crack-opening stress ratio near the initial crack length was caused by the lower constraint due to the hole. The crack-opening stress ratio reached nearly a constant level for most of the fatigue life. The rapid drop in the crack-opening stress ratio near the end of life was due to the crack rapidly growing to failure (yield zone became large compared to the uncracked ligament). However, the cold-worked and reamed hole simulation exhibited a much larger rise in the crack-opening stress ratio, reaching a value of 87% of the maximum applied stress. As shown in Figure 20(b), most of the fatigue life was consumed while the crack-opening stress ratio was at the high level.

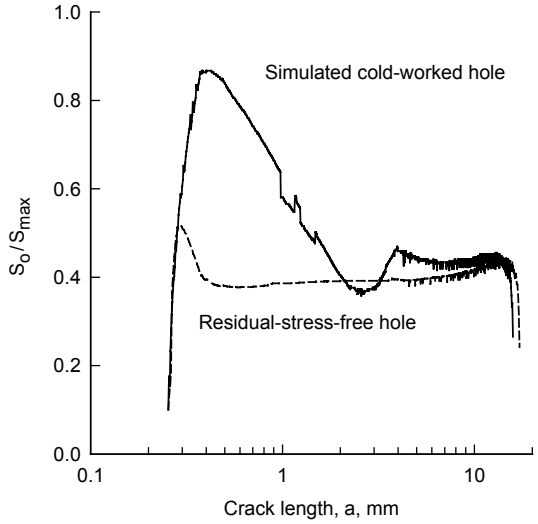

Figure 20(a) – Calculated crack-opening stress levels as a function of crack length during constant-amplitude loading for a residual-stress-free hole and a simulated cold-worked hole.

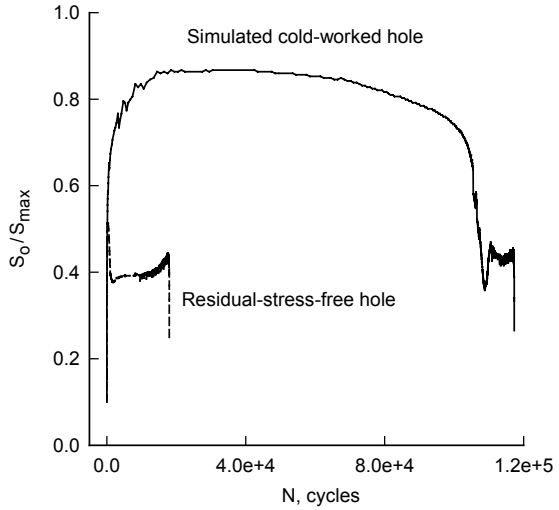

Figure 20(b) – Calculated crack-opening stress levels as a function of cycles during constant-amplitude loading for a residual-stress-free hole and a simulated cold-worked hole.

Concluding Remarks

The primary objective of this study was to enhance the FASTRAN crack-closure model to simulate the introduction of compressive residual stresses due to cold-worked and reamed holes. Cold-worked residual stresses were simulated by using a single overload on the crack-closure model to induce residual stresses at the edge of the hole that are similar to those from finite-element analyses. Several improvements were also made in the crack-closure model: (1) K-analogy was activated for all crack configurations to improve the transferability of the crack-opening stresses from the model to the actual crack configuration; (2) the plastic-zone region was composed of 20 elements to more accurately model the steep stress gradients in the residual-stress fields; (3) the hole or notch was assumed to control the constraint on the first load cycle and then later the crack controlled the constraint level, as in the original model; (4) the stress-intensity factor solution for a single crack at an open hole in a specimen subjected to remote uniform displacement was developed; (5) an option to ream a hole to remove plastically deformed material was incorporated into the model, and (6) an option to induce a cut or small notch at the edge of a hole to simulate the introduction of crack starters at the edges of holes.

The improved model was demonstrated on crack length versus cycles data generated from two test programs to study the influence of residual stresses on crack growth rate behavior on two materials. In the first program, compressive residual stresses were induced by a remote overload on a 2024 alloy, whereas, in the second program, the residual stresses were induced by cold working a hole and reaming on a 7075 alloy. Using the baseline effective stress-intensity factor range versus crack growth rate relationship for each material, predictions were made on the various test specimens. The comparison of measured and predicted crack length versus cycles behavior for the overload study agreed very well, except for an extreme case where it was suspected that the crack grew around the overload plastic zone. For the cold-worked hole case, the measured and predicted life from a small initial crack (0.25 mm) to failure was about 45% short of the average test lives. However, the residual stresses in the model were still not as large in magnitude as those calculated from the finite element model. Thus, the short life would be expected. But this study has provided an improved FASTRAN life-prediction model for durability and damage-tolerant life calculations for components that have various forms of residual stresses and has further verified that the crack-closure concept accounts for residual stresses on crack growth rate behavior.

References

1. Newman, J. C., Jr., "A Crack-Closure Model for Predicting Fatigue Crack Growth Under Aircraft Spectrum Loading," Methods and Models for Predicting Fatigue Crack Growth Under Random Load, ASTM STP 748,1981, pp. 53-84.

2. Newman, J. C., Jr., "FASTRAN-II - A Fatigue Crack Growth Structural Analysis Program," NASA TM 104159, February 1992.

3. Newman, J. C., Jr., "Prediction of Fatigue Crack Growth Under Variable Amplitude and Spectrum Loading Using a Closure Model," Design of Fatigue and Fracture Resistant Structures, ASTM STP 761, 1982, pp. 255-277.

4. Liu, A. F., "Crack Growth at a Preyielded Hole," *Journal of Engineering Materials and Technology*, Transactions of ASME, Vol. 104, 1982, pp. 153-154.

5. Liu, A. F., "The Effect of Residual Stresses on Crack Growth From a Hole," NOR 79-74, Northrop Corporation, Aircraft Group, Hawthorne, CA, August 1979.

6. LaRue, J., "The Effect of Residual Stress on Fatigue Crack Growth," M.S. Thesis, Mississippi State University, 2005.

7. Newman, J. C., Jr., "A Nonlinear Fracture Mechanics Approach to the Growth of Small Cracks," Behavior of Short Cracks in Airframe Components, AGARD Conference Proceedings No. 328, 1983, pp. 6.1-6.26.

8. Newman, J. C., Jr., Swain, M. H., and Phillips, E. P., "An Assessment of the Small-Crack Effect for 2024-T3 Aluminum Alloy," Small Fatigue Cracks, The Metallurgical Society, Inc., Warrendale, PA, 1986, pp. 427-452.

9. Swain, M. H., Everett, R. A., Newman, J. C., Jr., and Phillips, E. P., "The Growth of Short Cracks in 4340 Steel and Aluminum-Lithium 2090," AGARD R-767, 1990, pp. 7.1-7.30.

10. Newman, J. C., Jr., "Effects of Constraint on Crack Growth under Aircraft Spectrum Loading," Fatigue of Aircraft Materials, Delft, The Netherlands, Delft University Press, 1992, pp. 83-109.

11. Newman, J. C., Jr., Phillips, E. P., and Swain, M. H., "Fatigue-Life Prediction Methodology Using Small-Crack Theory," *International Journal of Fatigue*, Vol. 21, 1999, pp. 109-119.

12. Everett, R. A., Jr., Newman, J. C., Jr., and Phillips, E. P., "The Effects of Machining-Like Scratch on the Fatigue Life of 4340 Steel," *Proceedings of the American Helicopter Society, 55th Annual Forum*, Montreal, Quebec, Canada, May 25-27, 1999.

13. Elber, W., "The Significance of Fatigue Crack Closure," Damage Tolerance in Aircraft Structures, ASTM STP 486, American Society for Testing and Materials, Philadelphia, PA, 1971, pp. 230-242.

14. Lam, Y. C. and Lian, K. S., "Effect of Residual Stress and its Redistribution on Fatigue Crack Growth," *Theoretical Applied Fracture Mechanics*, Vol. 12, No. 1, 1989, pp. 59-66.

15. Dugdale, D. S., "Yielding of Steel Sheets Containing Slits," *Journal of the Mechanics and Physics of Solids*, Vol. 8, 1960, pp. 100-104.

16. McClung, R. C., "Finite-Element Analysis of Specimen Geometry Effects on Fatigue Crack Closure," *Fatigue and Fracture of Engineering Materials and Structures*, Vol. 17, 1994, pp. 861-872.

17. Chang, C. and Mear, M. E., "A Boundary-Element Method for Two-Dimensional Linear Elastic Fracture Analysis," *International Journal of Fracture*, Vol. 74, 1996, pp. 219-251.

18. Shivakumar, V. and Forman, R. G., "Green's Function for a Crack Emanating from a Circular Hole in an Infinite Sheet," *International Journal of Fracture*, Vol. 16, No. 4, 1980, pp. 305-316.

19. Isida, M., "Stress-Intensity Factors for the Tension of an Eccentrically Cracked Strip," Trans. ASME, Series E, *Journal of Applied Mechanics*, Vol. 33, 1965, p. 674.

20. Tada, H., Paris, P. C., and Irwin, G. R., "The Stress Analysis of Cracks Handbook," Third Edition, *American Society of Mechanical Engineers*, 2000, p.233.

21. NASGRO Reference Manual 4.02, Southwest Research Institute and NASA Johnson Space Center, 2002.

22. Hudson, C. M., "Effect of Stress Ratio on Fatigue-Crack Growth in 7075-T6 and 2024-T3 Aluminum Alloy Specimens," NASA TN D-5390, August 1969.

23. Newman, J. C., Jr., Wu, X. R., Venneri, S. L., and Li, C. G., "Small-Crack Effects in High-Strength Aluminum Alloys - A NASA/CAE Cooperative Program," NASA RP-1309, May 1994.

24. Phillips, E. P., "The Influence of Crack Closure on Fatigue Crack Growth Thresholds in 2024-T3 Aluminum Alloy," ASTM STP 982, 1988, pp. 505-515.

25. Newman, J. C., Jr., "A Crack Opening Stress Equation for Fatigue Crack Growth," *International Journal of Fracture*, Vol. 24, 1984, R131-R135.

26. Hudson, C. M. and Hardrath, H. F., "Effects of Changing Stress Amplitude on the Rate of Fatigue-Crack Propagation in Two Aluminum Alloys," NASA TN D-960, September 1961.

27. Pavier, M. J., Poussard, C., and Smith, D. J., "A Finite-Element Simulation of the Cold Working Process for Fastener Holes," *Journal of Strain Analysis*, Vol. 32, No. 4, 1997, pp. 287-300.

28.Rich, D. L. and Impellizzeri, L. F., "Fatigue Analysis of Cold-Worked and Interference Fit Fastener Holes," ASTM STP 637, 1975, pp. 153-175.